

# Polymer translocation through nanopores: Parking lot problems, scaling laws and their breakdown

R. Metzler<sup>a</sup> and K. Luo

Physics Department T30g, Technical University of Munich, 85747 Garching, Germany

Received 01 September 2010 / Received in final form 14 September 2010  
Published online 12 November 2010

**Abstract.** The passage of a polymer through a narrow pore is associated with the crossing of a significant free energy barrier. Both in nature and in single molecule experiments the polymer is typically driven through the pore. We here address two such driving modes: (i) the driving by binding proteins that prevent (partial) back-sliding through the pore; and (ii) the driving by a trans-membrane force. In case (i) we derive the effective force and show finite size effects due to the size of the binding proteins. In case (ii) we demonstrate the crossover from a slow, equilibrium driving to a non-equilibrium behaviour at fast driving.

## 1 Introduction

The passage of a long polymeric chain through a narrow pore is a recurring theme in biology [1]. Thus, messenger RNA and proteins need to cross small channels in the nuclear membrane, proteins are constantly passed through cell walls or the membranes of cell organelles such as mitochondria. Similarly, DNA is exchanged through cell walls, either for information transfer with other cells, or, when viruses inject their DNA into a cell. Moreover, the translocation process has been argued to have far-reaching technological potential, for instance, for rapid DNA sequencing, gene therapy, and controlled drug delivery [2–13].

Apart from the biological and technological relevance, polymer translocation is of fundamental interest in polymer physics and chemistry. While passing through a narrow pore the polymer's degrees of freedom are significantly reduced when compared to an unconstrained situation. As a function of the number of already translocated monomers, a natural reaction coordinate for this process, the polymer passage through the pore requires the chain to cross a free energy barrier. In most biological situations as well as in experiments or simulations one therefore applies a driving force across the pore. Typically this is chosen to be a trans-membrane force. In experiments, this is achieved by an electric field falling off mainly across the pore. The charged chains, such as single stranded DNA, experience the driving almost exclusively inside the pore. Here we do not consider charges but assume a general force acting on the

<sup>a</sup> e-mail: metz@ph.tum.de

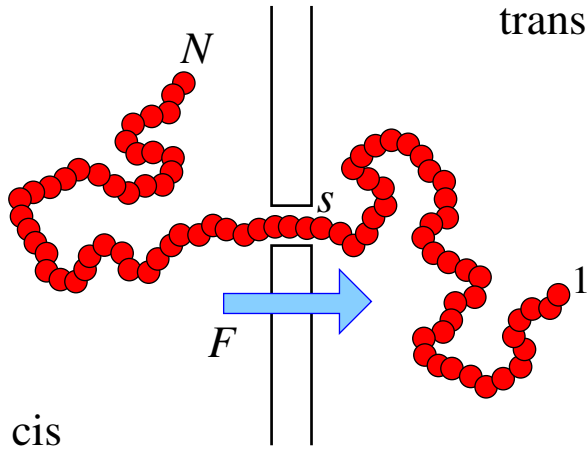


**Fig. 1.** Schematic of the translocation process. A chain with  $N$  monomers crosses a narrow pore. The reaction coordinate  $s$  measures the number of already translocated monomers.

monomer(s) inside the pore. Another possibility found in Nature, for instance for the transport of proteins across the mitochondrial membrane, is the driving in terms of the chemical gradient built up by binding proteins, that prevent (partial) back-sliding across the pore. In what follows we will address both mechanisms. We note that we neglect hydrodynamic interactions [12–16] as well as pore-chain interactions [17–20]. Albeit non-negligible effects, we concentrate on the statistical aspect due to the complexities of the binding proteins, and the polymeric aspects. As we will see, already these effects are interesting per se, and need to be understood before adding even higher complexity to the problem.

A schematic picture of the translocation process for a chain with  $N$  monomers is shown in Fig. 1. Here,  $s$  monomers of the chain have already crossed the membrane to the trans side, while  $N - s$  monomers are still located on the cis side of the pore. The arrow indicates the translocation direction due to the imposed boundary conditions, equivalent to the direction of the applied force  $F$  when present. We add the following initial and boundary conditions: at the beginning of the process, the first monomer is already threaded into the pore. In addition we assume a reflecting boundary condition for monomer 1 at the pore, i.e., we do not allow escape of the chain back to the cis side. Finally we impose an absorbing boundary condition at the right pore end for monomer  $N$ . Once all monomers have crossed the pore, that is, we stop the process and therefore determine the first crossing behaviour.

A free polymer chain consisting of  $N$  monomers may assume

$$\omega_{\text{free}}(N) \simeq \mu^N N^{\gamma-1} \quad (1)$$

configurations. Here  $\mu$  is the non-universal connectivity constant (e.g.,  $\mu = 6$  on a cubic lattice) and  $\gamma$  the configuration exponent. For a Gaussian chain  $\gamma = 1$  while for the case of a self-avoiding chain we have  $\gamma = 1.16$  in three dimensions [21]. Once the chain is attached to a wall with one end, the law in Eq.(1) involves a different scaling exponent,  $\gamma_1$ . In three dimensions,  $\gamma_1 = 0.680$  for a self-avoiding chain, i.e., as expected the wall prevents the polymer to assume all possible configurations. In our translocation scheme (compare Fig. 1) we have two parts of the chain connected to a wall on either side, such that the overall number of degrees of freedom for a given value of the translocation coordinate  $s$  assumes the form

$$\omega_{\text{transl}}(s) \simeq \mu^N (N - s)^{\gamma_1 - 1} s^{\gamma_1 - 1}. \quad (2)$$

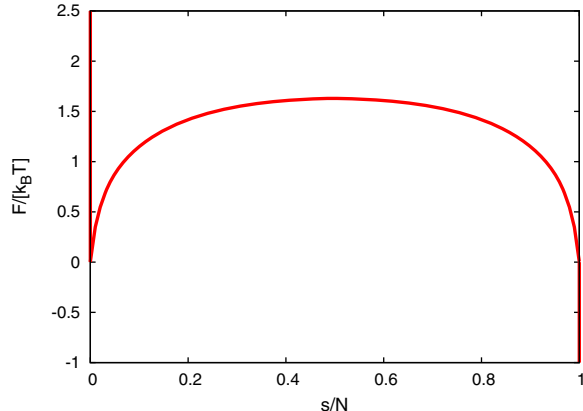


**Fig. 2.** Free energy barrier for the translocating chain as function of the reduced reaction coordinate  $s/N$ , in units of thermal energy  $k_B T$ . We chose the value  $\gamma_1 = 1/2$ .

The associated free energy becomes

$$\begin{aligned}\mathcal{F}(s) &= -k_B T \ln \omega_{\text{transl}}(s) \\ &\simeq -k_B T \left( N \ln \mu + (\gamma_1 - 1) \ln [(N-s)s] \right).\end{aligned}\quad (3)$$

This profile is shown in Fig. 2 in reduced coordinates. The vertical line to infinity at  $s = 0$  corresponds to the reflecting boundary condition, while the opposite vertical line at  $s = N$  represents the absorbing boundary condition terminating the translocation process. The barrier height corresponds to [22]

$$\Delta \mathcal{F}(N) = \mathcal{F}(N/2) - \mathcal{F}(1) = (1 - \gamma_1) k_B T \ln N.\quad (4)$$

For a flexible, self-avoiding chain with 200 monomers this corresponds to the modest barrier height of  $1.7k_B T$ , increasing to  $2.4k_B T$  for a chain with  $N = 2000$ .

## 2 Chaperone-driven translocation

One way of forcing the translocation process is through the presence of binding proteins, so-called chaperones (or chaperonins). As shown in Fig. 3, these chaperones bind to the chain-to-be-translocated and prevent (partial) backslicing of the chain. Typically one chaperone covers more than one monomer of the translocating chain. In general, chaperones of the same kind or of different types may be present on both sides of the pore. Then their respective concentration or binding affinity determines the direction of translocation. Here, we consider the simplest case, in which binding proteins are present on the trans side of the membrane. Once the chain is fully passed through the pore, the chaperones may be shaved off by competing processes, for instance, the folding of the translocated protein.

The fact that the chaperones cover several monomers of the chain-to-be-translocated gives rise to some interesting physical phenomena. Focusing on these we consider the simplified case of a stiff chain with lattice constant  $a$ , i.e., in this Section we neglect polymeric degrees of freedom of the translocating chain. We will come back to phenomena connected to the polymeric nature of the translocating chain in the next Section. Moreover, we here assume that the system is close to equilibrium.

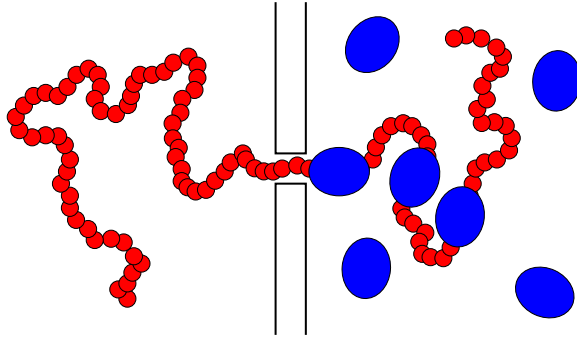


**Fig. 3.** Schematic of translocation driving by binding proteins (chaperones): Proteins transiently binding to the chain-to-be-translocated prevent partial back-sliding through the pore. The chaperones typically cover several monomers of the polymer.

With these assumptions we describe the translocation in terms of the partition coefficient  $\mathcal{Z}(s, n)$ , where  $s$  is the number of already translocated monomers, and  $n$  counts the number of chaperones bound to the translocating chain. The partition function is therefore [23–25]

$$\mathcal{Z} = \sum_{s,n} \mathcal{Z}(s, n), \quad (5)$$

and at stationarity the probability distribution to measure  $s$  translocated monomers and  $n$  bound chaperones is given in terms of

$$P_{\text{st}}(s, n) = \frac{\mathcal{Z}(s, n)}{\mathcal{Z}}. \quad (6)$$

The binding strength  $\kappa = c_0 K_{\text{eq}}$  per chaperone is given in terms of the chaperone concentration  $c_0$  in the ambient volume and the binding constant  $K_{\text{eq}}$ . The latter can be written as  $K_{\text{eq}} = v_0 \exp(\beta|\varepsilon_{\text{bind}}|)$  with the typical chaperone volume  $v_0$  and the binding energy  $\varepsilon_{\text{bind}}$ . The constant  $\beta = 1/(k_B T)$  is the Boltzmann factor.

In how many ways can we arrange the chaperones on the  $s$  monomers present on the trans side? If each chaperone occupies  $\lambda$  monomers these complexions are given by the factor [26, 27]

$$\Omega = \binom{s - (\lambda - 1)n}{n} = \frac{[s - (\lambda - 1)n]!}{n!(s - \lambda n)!}. \quad (7)$$

The binding chaperones therefore enter the partition factor  $\mathcal{Z}(s, n)$  in the form

$$\mathcal{Z}(s, n) = \kappa^n \Omega(s, n). \quad (8)$$

The corresponding force on the translocating chain can then be expressed as [23, 24]

$$\frac{F(s)}{a} = k_B T \frac{1}{\mathcal{Z}_{\text{red}}} \sum_n \frac{\partial}{\partial s} \mathcal{Z}(s, n), \quad (9)$$

where  $\mathcal{Z}_{\text{red}}(s) = \sum_{n=0}^{n_{\max}(s)} \mathcal{Z}(s, n)$ , and  $n_{\max}(s) = \max\{s/\lambda\}$  is the maximum number of bound chaperones for given value of  $s$ . The functional dependence of the force  $F$  versus the number  $s$  of already translocated monomers is shown in Fig. 4. For small chaperones,  $\lambda = 1$ , we observe a relatively quick saturation to a stationary value.

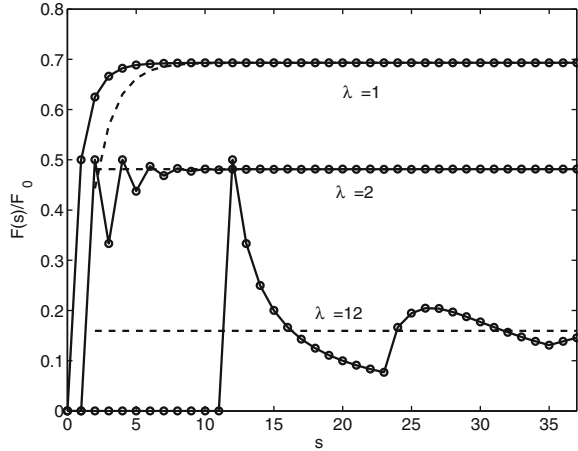


**Fig. 4.** Driving force  $F(s)$  in units of  $F_0 = k_B T/a$  ( $a$  is the monomer size of the chain-to-be-translocated) as function of the number  $s$  of already translocated monomers. For chaperone size  $\lambda > 1$  monomer we observe distinct oscillations stemming from the “parking lot problem”, see text. We chose the binding strength  $\kappa = 1$ .

When the chaperones cover more than one monomer we observe distinct oscillations: the force remains zero until  $\lambda$  monomers have translocated, providing the necessary chain length for the first chaperone to bind. After the first chaperone is bound, the translocating chain needs to move another  $\lambda$  monomers through the pore, before the second chaperone can bind, and so forth. Another subtlety arising in this context is the parking-lot problem [28–30]: if the proteins do not bind directly head-to-tail, the remaining gap between two such proteins may be too small for another protein to bind and thus stays vacant. Therefore, the larger the chaperone, the lower the resulting effective force.

The dynamics of this chaperone-driven translocation can be quantified in terms of a master equation of the type [23–25]

$$\begin{aligned} \frac{\partial}{\partial t} P(s, n, t) = & k^+(s-1, n)P(s-1, n, t) + k^-(s+1, n, t)P(s+1, n, t) \\ & - [k^+(s, n) + k^-(s, n)]P(s, n, t) \\ & + r^+(s, n-1)P(s, n-1, t) + r^-(s, n+1)P(s, n+1, t) \\ & - [r^+(s, n) + r^-(s, n)]P(s, n, t) \end{aligned} \quad (10)$$

for the probability density  $P(s, n, t)$  to find  $s$  translocated monomers with  $n$  bound chaperones at a given time  $t$ . The transfer rates  $k$  and  $r$  are defined through the partition coefficients. In particular, the forward rate for the chain through the pore is not influenced by the chaperones and therefore given by the constant rate

$$k^+(s, n) = k. \quad (11)$$

In contrast, the backward rate  $k^-$  is given by

$$k^-(s, n) = k \frac{\mathcal{Z}(-, )}{\mathcal{Z}(, )} = k \frac{\Omega(s-1, n)}{\Omega(s, n)}, \quad (12)$$

as dictated by the detailed balance condition and Eq. (11). The backward rate in Eq. (12) thus corresponds to the diffusive forward rate  $k$  times the probability that

the binding site closest to the pore is vacant. Note that in the limit  $n = 0$ ,  $\Omega(s-1, 0) = \Omega(s, 0)$ , and thus forward and backward rates become the same. Similarly, the rates for chaperone binding and unbinding are given by the relations

$$r^+(s, n) = q(n+1) \frac{\mathcal{Z}(s, n+1)}{\mathcal{Z}(s, n)} = q\kappa \frac{(n+1)\Omega(s, n+1)}{\Omega(s, n)} \quad (13)$$

and

$$r^-(s, n) = nq. \quad (14)$$

Thus, while the unbinding of a chaperone is simply proportional to the overall number of bound chaperones,  $n$ , times the unbinding rate  $q$ , the binding of an additional chaperone depends on the number of ways

$$\mathcal{N} = (n+1) \frac{\Omega(s, n+1)}{\Omega(s, n)} \quad (15)$$

this chaperone can be added. As for the force, we observe the parking lot effect for chaperones that occupy more than one monomer: if there are less than  $\lambda$  monomers between two already bound chaperones, no additional chaperone can bind. Also the binding/unbinding rates for the chaperones fulfil detailed balance. After definition of the appropriate initial and boundary conditions, the master equation can be solved numerically. We can, however, distinguish some interesting limiting cases:

## 2.1 Slow chaperone binding: diffusive translocation dynamics

The binding of chaperones becomes slow when either the volume concentration  $c_0$  of chaperones is low, or when their binding energy  $|\varepsilon_{\text{bind}}|$  is small. On not too long time scales, starting with a bare chain emerging from the pore, the dynamics is exclusively described by the two transfer rates  $k^+(s, 0) = k^-(s, 0) = k$ . That is, forward and backward rates become equal, causing a purely diffusive translocation of the chain. It can be shown that the translocation time scales like [23, 24]

$$\tau_{\text{diff}} = k^{-1} \left[ (N+1) \left( 1 + \frac{N}{2} \right) \right] \sim \frac{N^2}{2k} = \frac{L^2}{2D_0}. \quad (16)$$

In the last step we identified the chain length  $L = Na$  and the diffusion coefficient  $D_0 = a^2 k$ . The diffusive case corresponds to the slowest possible case of translocation in this scheme.

## 2.2 Fast binding and slow unbinding: ratchet motion

In the opposite case of fast binding but slow unbinding we encounter the limiting case of ratchet motion for small chaperones ( $\lambda = 1$ ). On not too long time scales this motion corresponds to the transfer rates  $k^+(s) = k$  and  $k^-(s) = 0$ . Due to the fast, irreversible binding of chaperones, that is, the chain cannot slide backwards. Our master equation reduces to the effective equation

$$\frac{\partial}{\partial t} \bar{P}(s) = k \left( \bar{P}(s-1, t) - \bar{P}(s, t) \right) \approx -k \frac{\partial}{\partial s} \bar{P}(s, t), \quad (17)$$

where the  $\approx$  sign corresponds to the continuum approximation of the discrete equation, from which we see that the motion corresponds to one of the two propagation

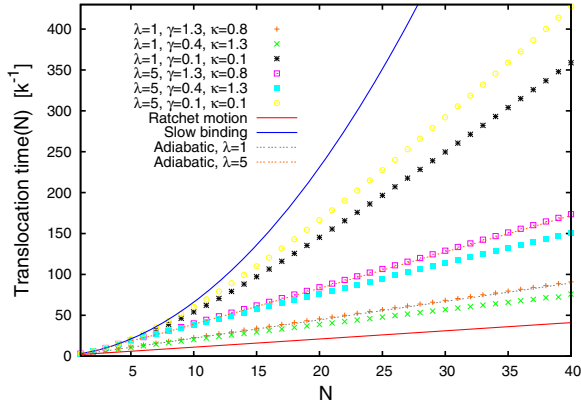


**Fig. 5.** Mean translocation time as function of chain length  $N$  in the case of chaperone-driven chain passage. The linear increase with  $N$  in the ratchet case is distinct. We use the abbreviation  $\gamma = q/k$  for the ratio of the chaperone unbinding rate  $q$  and chain monomer diffusion rate  $k$ .

modes of the wave equation. The resulting motion is therefore ballistic. From the discrete equation we obtain the translocation time

$$\tau_{\text{ratch}} = \frac{N+1}{k} = \frac{2}{N} \tau_{\text{diff}}. \quad (18)$$

The ratchet limit corresponds to the fastest possible translocation scenario of chaperone-driven chain passage. For larger chaperones ( $\lambda > 1$ ) the ratcheting effect becomes reduced by the parking lot effect, i.e., each time a chaperone binds, the chain needs to diffuse another  $\lambda$  monomers, before another chaperone is able to bind.

### 2.3 Fast chaperone binding and unbinding: adiabatic elimination

When both binding and unbinding of chaperones become fast, we can adiabatically eliminate the fast variable  $n$ , the number of chaperones bound at a given time. The associated mean translocation time then becomes

$$\tau_{\text{adiab}} = k^{-1} \sum_{s=0}^N \frac{1}{\mathcal{Z}(s)} \sum_{s'=0}^s \mathcal{Z}(s'), \quad (19)$$

where, as before,  $\mathcal{Z}(s) = \sum_{n=0}^{n_{\max}(s)} \mathcal{Z}(s, n)$  and the maximum number of bound chaperones for given  $s$  is  $n_{\max}(s) = \max\{s/\lambda\}$ . Concrete evaluations are then carried out numerically.

Figure 5 shows the mean translocation time for the chaperone-driven translocation problem. The large range of associated time scales is distinct. The labels “adiabatic” refer to the adiabatic approximation described above.

## 3 Polymer translocation dynamics and trans-membrane force

In the above considerations we neglected the polymeric degrees of freedom of the translocating chain and concentrated on the effect of the chaperones that partially rectify the passage of the chain. For relatively short chains, in particular, for chains

with a considerably high persistence length, this approach is justified. What happens when we consider a sufficiently long and flexible polymer chain? We review here some arguments that in this case the translocation dynamics indeed becomes anomalous. After presenting results from various groups, leading to different claims about the associated dynamic scaling exponents, we show that the conflicting results can in fact be reconciled.

The first approaches to model chain translocation in absence and presence of a trans-membrane force were based on a standard Kramers transition approach using the entropic barrier in Eq. (3), assuming friction to be independent of  $N$  [31, 32]. In this continuum approach it is assumed that the probability density  $P(s, t)$  for finding  $s$  translocated monomers at time  $t$  fulfills the continuity equation

$$\frac{\partial}{\partial t} P(s, t) = -\frac{\partial}{\partial s} j(s, t), \quad (20)$$

and the probability current  $j(s, t)$  combines a diffusive term with diffusion constant  $D = \frac{\mu}{k_B T}$ , and a drift term in which the force is given by the negative gradient of the free energy profile in Eq. (3):

$$j(s, t) = -D \left( \frac{\partial}{\partial s} P(s, t) + \frac{P(s, t)}{k_B T} \frac{\partial}{\partial s} \mathcal{F}(s) \right). \quad (21)$$

Combining these two equations, we obtain the Fokker-Planck equation

$$\frac{\partial}{\partial t} P(s, t) = \frac{\partial^2}{\partial s^2} P(s, t) + (\gamma_1 - 1) \frac{\partial}{\partial s} \frac{1-2s}{(1-s)s} P(s, t), \quad (22)$$

in which we rescaled the variables à la  $s \rightarrow sN$  and  $t \rightarrow tD/N^2$  [33]. From this equation we see that the resulting scaling for the mean translocation time with chain length is  $\tau \simeq N^2$  for unbiased translocation. In presence of a constant external driving we may neglect the entropic drift term, and the scaling of the mean translocation time changes to  $\tau \simeq N$ .

Can such a simple scenario work? The Rouse equilibration time of a free polymer chain can be estimated as the time it takes the chain to diffuse over a range of the gyration radius  $R_g$  (root mean squared extension):

$$\tau_R \simeq \frac{R_g^2}{D_{\text{c.o.m.}}} \simeq \frac{R_g^2 N}{D_{\text{mon}}} \simeq \frac{N^{1+2\nu}}{D_{\text{mon}}}, \quad (23)$$

where  $D_{\text{c.o.m.}} \simeq D_{\text{mon}}/N$  is the centre-of-mass diffusivity and  $D_{\text{mon}}$  the diffusion constant for a monomer. The Flory exponent  $\nu$  acquires the values  $\nu = 1/2$  for a phantom chain, and  $\nu(2D) = 0.75$  and  $\nu(3D) = 0.588$  for a self-avoiding chain in two and three dimensions, respectively [21]. Therefore, the Rouse time scales like  $\tau_R \simeq N^2/D_{\text{mon}}$  for a Gaussian chain, which would be marginally consistent with the above Kramers barrier crossing picture. However, the same picture can no longer be correct for a self-avoiding polymer, as the translocation time would be shorter than the Rouse equilibration time  $\tau_R$  [33]. The chain passing through a narrow pore should not be faster than a freely diffusing chain. This paradox renders the concept of equilibrium entropy and the ensuing picture of normally diffusive entropic barrier crossing inappropriate for the polymeric translocation dynamics. From numerical analysis in 2D it was indeed shown that the translocation time scales like  $\tau \simeq N^{1+2\nu}$ : the translocation time scales exactly like the equilibration time, but with a considerably larger prefactor [33]. This result was recently corroborated in 2D and 3D by extensive numerical

simulations based on the Fluctuating Bond [34] and Langevin Dynamics models with the bead-spring approach [35–37].

What does this imply for the free translocation dynamics? Let us follow the scaling argument of Chuang et al. [33]: assume the Flory scaling of the gyration radius,  $R_g \simeq N^\nu$  and assume further that the chain relaxation time is of the Rouse type,  $\tau_R \simeq N^{1+2\nu}$ . The progress of the translocation process will follow a scaling law with dynamic exponent  $\zeta$ :  $\langle \Delta s^2(t) \rangle \simeq t^{2\zeta}$ . At the total chain translocation time  $\tau$  we should reach the value  $N^2 \simeq \langle \Delta s^2(\tau) \rangle \simeq \tau^{2\zeta} \simeq N^{2\zeta(1+2\nu)}$  of the diffusion variance. Thus we identify the dynamic exponent  $\zeta = 1/(1 + 2\nu)$ , whose values are  $\zeta = 1/2$  for phantom chains, and  $\zeta(2D) = 0.4$  and  $\zeta(3D) \approx 0.46$  for self-avoiding chains, respectively. Thus, while Gaussian chains according to this scaling argument indeed diffuse normally, in the case of self-avoiding chains the resulting diffusion

$$\langle \Delta s^2(t) \rangle \simeq t^\alpha, \quad \alpha = 2\zeta, \quad (24)$$

is subdiffusive, characterised by the anomalous diffusion exponent  $\alpha < 1$ . It was suggested that such subdiffusive dynamics could be modelled in terms of a fractional Fokker-Planck equation [22, 38, 39].

For driven translocation the deviation from equilibrium is expected to be even more pronounced, while the equilibrium entropic barrier becomes less relevant for the translocation dynamics. In this case, a lower bound  $\tau \simeq N^{1+\nu}$  was estimated for the translocation time [40]. Lattice Monte Carlo (MC) simulations of self-avoiding chains in 2D revealed  $\alpha \approx 1.5$  [40], which is smaller than  $1 + \nu = 1.75$ , a difference attributed to finite size effects. However, additional simulation studies found a crossover from  $\tau \sim N^{1.46 \pm 0.01} \approx N^{2\nu}$  for relatively short polymers to  $\tau \sim N^{1.70 \pm 0.03} \approx N^{1+\nu}$  for longer chains ( $N > 200$ ) using Fluctuating Bond [41] and Langevin Dynamics [35, 42] models in 2D. Increasing the friction, the crossover vanished and only the exponent  $1 + \nu$  was observed [35]. The crossover is absent in 3D for long chains ( $N \sim 800$ ) and  $\alpha \approx 1.40$  is observed using both Langevin Dynamics [43] and GROMACS molecular dynamics simulations with Langevin Dynamics thermostats [44]. Lehtola et al. [45] find approximately the same exponent of about 1.40 based on Langevin Dynamics simulations, however, their exponent increases with increasing force, which cannot hold asymptotically. Finally, Gauthier and Slater [46] reported  $\tau \sim N^{1+\nu}$  using an exact numerical method valid at low bias.

Recently, however, alternative scaling scenarios have been presented in Refs. [47, 48] that contradict above results. These two views also disagree with each other [49]. To resolve the apparent discrepancy on the value of  $\alpha$  for driven translocation, we performed high-accuracy Langevin Dynamics simulations on the behaviour of  $\tau \simeq N^\alpha$  as a function of  $N$  [50], see the Appendix for details. As main result we find that there exist two limiting regimes, corresponding to slow and fast translocation. The slow translocation case is realised for low driving forces and/or high friction, and in this regime we find that indeed  $\alpha \approx 1 + \nu$ . In the opposite limit of fast translocation for high driving forces and/or low friction, the corresponding scaling exponent changes to  $\alpha \approx 1.37$ . We provide evidence that the difference between the scaling exponents for these two regimes can be ascribed to the highly deformed chain conformation during fast translocation, reflecting a pronounced non-equilibrium situation.

Figure 6 shows the scaling of the translocation time with chain length  $N$ . Indeed, we observe two distinct scaling regimes. At high friction or low driving force the motion is governed by the dynamic scaling exponent  $\alpha \approx 1 + \nu \approx 1.588$ . These exponents are in good agreement, not only with the prediction  $1 + \nu$  from Refs. [40, 51], but also with the results from the exact numerical method reported in Ref. [46] for low fields, as well as with our previous 2D simulations for relatively long polymers [35, 41, 42]. However, when the dynamics get faster, either by decreasing the friction

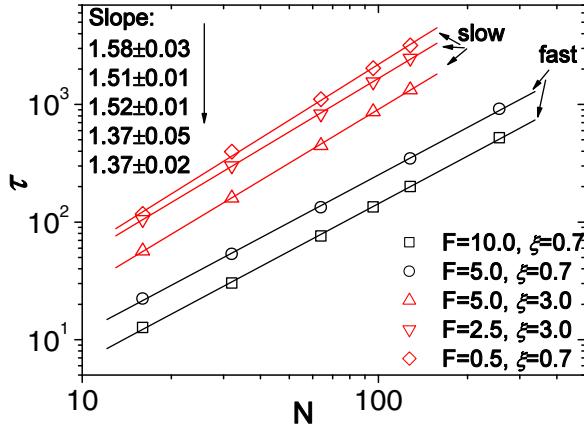


**Fig. 6.** Translocation time  $\tau$  versus chain length  $N$  for driven translocation in three dimensions, with varying trans-membrane force  $F$  and friction coefficient  $\xi$ . For fast translocation the scaling exponent is  $\alpha \approx 1.37$  while for slow translocation we observe  $\alpha \approx 1 + \nu$  expected from equilibrium arguments.

or increasing the driving force, deviations from this prediction become obvious, and the exponent decreases to  $\alpha \approx 1.37$ , consistent with the predictions from Ref. [47], see below. The latter exponent is also in agreement with previous results [43, 44, 52] and the recent experimental findings for individual short DNA molecules in the range  $150 \sim 3500$  bps through solid-state nanopores [6]. These observations demonstrate that there exist two limiting dynamic regimes as demonstrated in Fig. 6: slow and fast translocation. For slow translocation,  $\alpha \approx 1 + \nu$ , while  $\alpha \approx 1.37$  for fast translocation.

In the scaling arguments presented in Ref. [40], an essential assumption is that the chain is not severely deformed (i.e., assuming close-to-equilibrium configurations) during the translocation process. For slow translocation, these assumptions are satisfied. Not surprisingly the predicted exponent  $1 + \nu$  is observed in this regime, in contrast to the fast dynamics regime claimed in Ref. [45]. For fast translocation the chain is highly deformed and the translocation dynamics is different.

Based on the fractional Fokker-Planck equation involving long-range memory effects the scaling  $\alpha = 2\nu + 1 - \gamma_1$  was obtained, such that  $\alpha = 1.55$  in 2D and 1.5 in 3D (here  $\gamma_1 \approx 0.945$  in 2D and  $\approx 0.68$  in 3D is the critical surface exponent) [48]. The Monte Carlo simulations in Ref. [48] were carried out for weak driving forces, producing  $\tau \sim N^{1.5}/F$  in 3D, in excellent agreement with the value  $\tau \sim N^{1+\nu}/F$  for slow translocation processes.

Using linear response theory with memory effects [49], Vocks et. al. [47] came up with the alternative estimate  $\tau \sim N^{\frac{1+2\nu}{1+\nu}}$  for 3D, which means  $\alpha = 1.37$  in 3D. Their  $\alpha$  in 3D is consistent with our numerical data for fast translocation. However, their estimate fails to capture the scaling exponent for slow translocation.

For the driven translocation experiments with a voltage applied across the pore, the force  $F$  acts only on the few monomers inside the pore. As a consequence, it was argued [40] that the centre of mass of the polymer should move with a velocity  $v \sim F/N$ . Thus the lower bound for the translocation time of an unhindered polymer is the time to move the distance  $R_g$ , giving rise to the scaling  $\tau \sim R_g/v \sim N^{1+\nu}/F$ . Figure 7 shows the translocation velocity  $v$  as function of the polymer length for different driving forces and friction coefficients,  $v \sim N^\delta$ . Here  $v$  is the average velocity with respect to the last monomer and we checked that the corresponding  $v$  of the centre of mass scales in the same way. For slow translocation, we indeed find

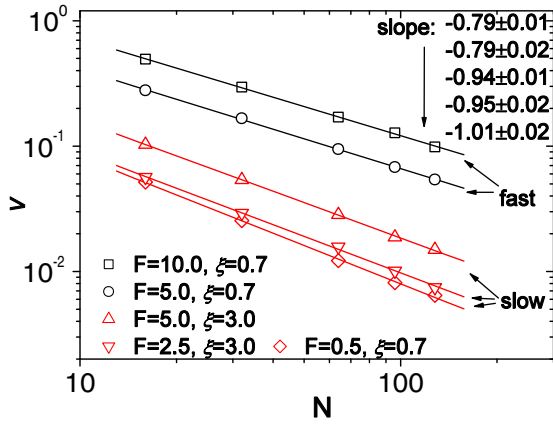


**Fig. 7.** Scaling of translocation velocity with chain length.

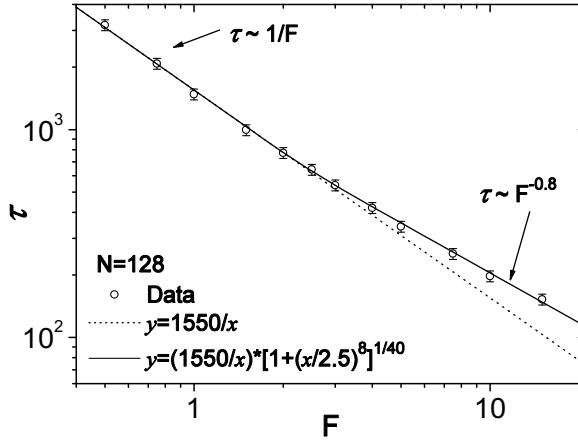


**Fig. 8.** Translocation time  $\tau$  versus driving force at  $\xi = 0.7$ . The solid line shows the empirical fit function defined in the graph.

$\delta \approx -1.0$ . In contrast, for fast translocation the velocity decreases less rapidly with  $N$ :  $\delta = -0.7 \dots 0.8$ , as also observed in Ref. [43]. We also studied how the translocation time varies as a function of the driving force for  $\xi = 0.7$  and  $N = 128$ , the result being displayed in Fig. 8. As long as  $F \leq 2$  we observe  $\tau \sim 1/F$ , before crossing over to  $\tau \sim F^{-0.80}$  for strong driving.

The difference of the translocation dynamics in the two regimes can be understood by inspecting the polymer configurations during the translocation process. For faster translocation, only part of the chain on the cis side manages to respond immediately, while the remaining part closer to the chain end does not yet feel the influence of the force. Thus, part of the chain on the cis side is deformed to trumpet or even stem-and-flower shapes [52]. Conversely, the translocated portion on the trans side has a fairly compact shape, as it does not have time to diffuse away from the pore exit. Along with a configuration close to equilibrium, Fig. 9 shows the shape of the chain under fast translocation conditions. The trumpet shape on the cis side as well as the quite compact configuration on the trans side appear distinct. These qualitative observations for such a typical chain configuration are more quantitatively analysed in terms of the gyration radius [50]. Indeed, for slow translocation we observe the typical equilibrium scaling  $R_g \sim N^{0.6}$  for the chain on the trans side right

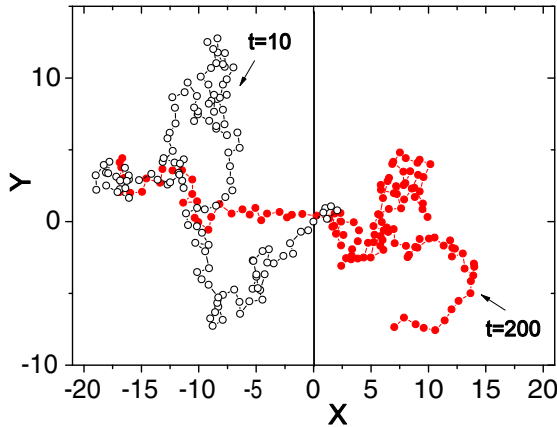


**Fig. 9.** Typical chain conformation during fast translocation for  $N = 128$ ,  $\xi = 0.7$ , and  $F = 5.0$ . 3D conformations are projected onto the XY plane. Black: early stage. Red: Later stage.

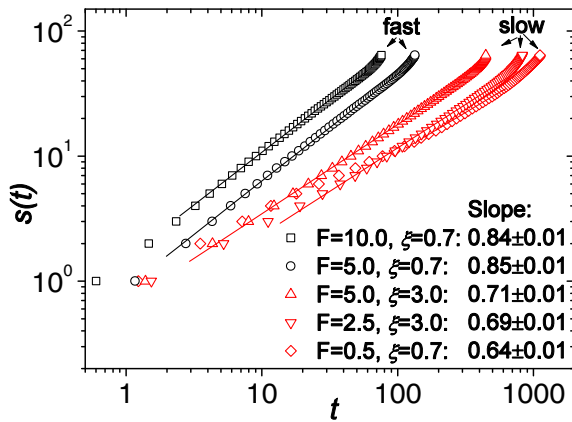


**Fig. 10.** The translocation coordinate as a function of time for different driving forces and friction coefficients, for  $N = 64$ .

after the translocation. In contrast, for fast translocation this scaling changes to the significantly different behaviour  $R_g \sim N^{0.51}$  reminiscent of a dense chain. As at equilibrium, the chain assumes the self-avoiding chain exponent  $\nu = 0.588$ , close to the measured exponent for slow translocation, the significant deviation from this value for fast translocation corroborates our claim that the chain does not attain equilibrium.

Finally the translocation coordinate is shown to follow the dynamic scaling  $\langle s(t) \rangle \simeq t^\beta$  for  $N = 64$  for different  $F$  and  $\xi$  in Fig. 10. For fast translocation we find  $\beta \approx 0.85$ , contrasting exponents around  $\beta \approx 0.6 \dots 0.7$  when translocation is slow. The occurrence of different values for  $\beta$  in fast versus slow translocation processes again shows the existence of different dynamic regimes. The definition  $\langle s(t) \rangle \simeq t^\beta$  implies that  $N \simeq \tau^\beta$ . Compared with  $\tau \simeq N^\alpha$ , one obtains  $\alpha\beta = 1$  if equilibrium arguments should hold. Indeed for  $F = 0.5$  and  $\xi = 0.7$ ,  $\alpha\beta = 1.01$ , which indicates that non-equilibrium effects do not appear to be severe. However,  $\alpha\beta = 1.16$  for  $F = 5.0$  and  $\xi = 0.7$  indicating a breakdown of our simple scaling due to pronounced non-equilibrium effects.

## 4 Discussion

Translocation of oligomeric and polymeric chains through narrow pores across a membrane is a ubiquitous phenomena in and across biological cells. Moreover, this process has numerous applications in technology. The complete process depends on numerous effects ranging from chain-pore interactions over charge effects to hydrodynamic interactions. However, even the complete understanding of the simple case of bare flexible polymer translocation remains formidable.

Here we considered two cases of translocation. First we addressed the case of a stiff (or short) chain for which polymeric degrees of freedom do not come into play. Instead we considered the effect of binding proteins that (partially) rectify the motion. As usually such proteins are larger than a single monomer of the chain-to-be-translocated the resulting effective force shows pronounced oscillations, corresponding to the parking lot effect: if the gap between here already bound proteins is too small, another protein cannot bind to the unoccupied monomers in this gap. Depending on the efficiency of the binding and unbinding dynamics the effective motion of the translocating chain can range from purely diffusive dynamics, for which the translocation time scales like the square of the chain length,  $\tau \simeq N^2$ , to ballistic ratchet motion with  $\tau \simeq N$ . Generalising the scheme we presented one may consider binding proteins of different chemical properties on both cis and trans side. Moreover it is possible to include cooperativity effects between vicinal chaperones, as well as the diffusion of binding chaperones along the chain.

Second we reinvestigated the case of a transmembrane force driving a polymeric chain through the pore. We showed that previous equilibrium assumptions used to derive the associated scaling exponents break down at sufficiently fast translocation, corresponding to high driving force and/or low friction. Above a threshold the chain configurations on both cis and trans sides deviate from the ones of a relaxed self-avoiding chain. On the cis side the tension successively propagates along the chain, creating a trumpet-like shape. On the trans side the chain does not manage to diffuse away from the pore quickly enough, such that a dense, almost compact configuration arises. The nonequilibrium behaviour accompanies all aspects of the translocation. Fast and slow translocation are characterised by different scaling regimes for the translocation time and velocity as functions of the chain length, the translocation time-driving force relation, as well as the scaling of the first moment of the translocation coordinate as a function of time. While slow translocation is consistent with previous scaling approaches as well as the fractional Fokker-Planck equation approach, for fast translocation these models break down. Instead, a model with pronounced memory on the level of the stochastic equation appears consistent with our simulations results.

Apart from the above geometry, in which both cis and trans side are unlimited halfspaces, other geometries are of interest when one considers applications in biology and technology. We show a few examples in Fig. 11. Thus, the translocation may be forced purely by entropy when the chain is originally confined. This can be due to a finite volume such as in the capsid of a virus [53], or the transversal confinement between two parallel walls, as shown in Fig. 11 (a) and considered in Ref. [54]. The opposite case of forcing the chain into a confined space can be important for technological applications, for instance, when effects of transversal confinement on polymeric chains are studied (case (b)). Similarly, one may study the translocation of an unconfined chain into a narrow fluidic channel. As shown in part (c), this could be achieved by sucking the chain into the channel simply by dragging it along a flow inside the channel. Cases (b) and (c) are investigated in forthcoming work [55–57].

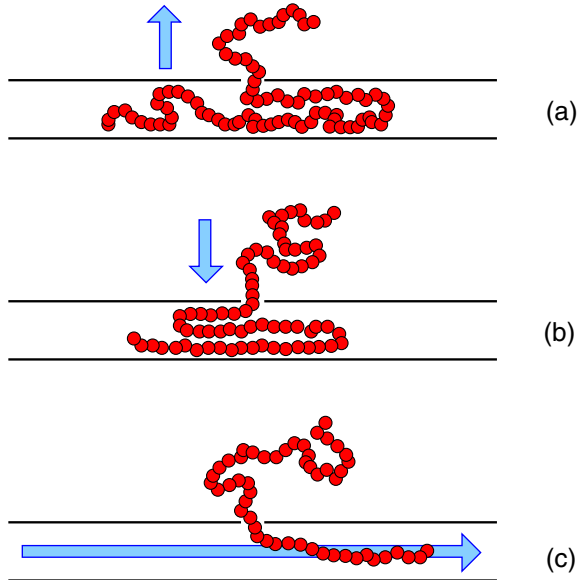


**Fig. 11.** Different translocation geometries. The arrow indicates the direction of the translocation force. (a) Translocation out of confinement is driven by the entropic pressure of the confined chain. Conversely, to feed the chain into a confined environment, we can either (b) apply a trans-membrane force or (c) use a longitudinal drag.

### Simulations details

In our simulations, the polymer chains are modeled as bead-spring chains of Lennard-Jones (LJ) particles with the Finite Extension Nonlinear Elastic (FENE) potential. Excluded volume interaction between monomers is modeled by a short range repulsive LJ potential:  $U_{LJ}(r) = 4\epsilon[(\frac{\sigma}{r})^{12} - (\frac{\sigma}{r})^6] + \epsilon$  for  $r \leq 2^{1/6}\sigma$ , and 0 for  $r > 2^{1/6}\sigma$ . Here,  $\sigma$  is the monomer diameter and  $\epsilon$  is the potential depth. The connectivity between neighboring monomers is modelled as a FENE spring with  $U_{FENE}(r) = -\frac{1}{2}kR_0^2 \ln(1 - r^2/R_0^2)$ , where  $r$  is the distance between consecutive monomers,  $k$  the spring constant, and  $R_0$  the maximally allowed separation between connected monomers. The wall (“membrane”) carrying the pore of diameter  $2\sigma$  is composed of particles of diameter  $\sigma$ . The wall thickness is  $\sigma$ . Between all monomer-wall particle pairs, there exists the same short range repulsive LJ interaction as described above.

In LD simulations each monomer is subject to conservative, frictional, and random forces:  $m\ddot{\mathbf{r}}_i = -\nabla(U_{LJ} + U_{FENE}) - \xi\dot{\mathbf{r}}_i + \mathbf{F}_{ext} + \mathbf{F}_i^R$  [58], where  $m$  is the monomer mass,  $\xi$  the friction coefficient, and  $\mathbf{F}_i^R$  the random force, that satisfies the fluctuation-dissipation theorem. The external force is expressed as  $\mathbf{F}_{ext} = F\hat{x}$ , where  $F$  is the external force strength exerted on the monomers in the pore, and  $\hat{x}$  is a unit vector in the direction along the pore axis. In the simulation, we use the LJ parameters  $\epsilon$  and  $\sigma$ , and the monomer mass  $m$  to fix the energy, length, and mass scales. This sets the time scale  $t_{LJ} = (m\sigma^2/\epsilon)^{1/2}$ . The dimensionless parameters in our simulations are  $R_0 = 2$ ,  $k = 7$ ,  $k_B T = 1.2$ . The Langevin equation is integrated in 3D.

Initially, the first monomer of the chain is placed in the entrance of the pore, while the remaining monomers evolve in the Langevin thermostat to obtain an equilibrium configuration. The translocation time is defined as the time interval between the entrance of the first segment into the pore and the exit of the last segment. Typically, we average our data over 1000 independent runs.

We acknowledge financial support from the Deutsche Forschungsgemeinschaft.

## References

1. B. Alberts, D. Bray, J. Lewis, M. Raff, J.D. Watson, *Molecular Biology of the cell* (Garland, New York, NY, 1994)
2. J.J. Kasianowicz, E. Brandin, D. Branton, D.W. Deamer, Proc. Natl. Acad. Sci. USA **93**, 13770 (1996)
3. S.E. Henrickson, M. Misakian, B. Robertson, J.J. Kasianowicz, Phys. Rev. Lett. **85**, 3057 (2000)
4. A. Meller, L. Nivon, D. Branton, Phys. Rev. Lett. **86**, 3435 (2001)
5. A. Meller, J. Phys. Cond. Mat. **15**, R581 (2003)
6. M. Wanunu, J. Suntin, B. McNally, A. Chow, A. Meller, Biophys. J. **95**, 1193 (2008)
7. A.J. Storm, C. Storm, J.H. Chen, H. Zandbergen, J.F. Joanny, C. Dekker, Nano Lett. **5**, 1193 (2005)
8. U.F. Keyser, B.N. Koeleman, S. van Dorp, D. Krapf, R.M.M. Smeets, S.G. Lemay, N.H. Dekker, C. Dekker, Nature Phys. **2**, 473 (2006)
9. A. Aksimentiev, J.B. Heng, G. Timp, K. Schulten, Biophys. J. **87**, 2086 (2004)
10. J.B. Heng, C. Ho, T. Kim, R. Timp, A. Aksimentiev, Y.V. Grinkova, S. Sligar, K. Schulten, G. Timp, Biophys. J. **87**, 2905 (2004)
11. J. Mathé, A. Aksimentiev, D.R. Nelson, K. Schulten, A. Meller, Proc. Natl. Acad. Sci. USA **102**, 12377 (2005)
12. M.G. Gauthier, G.W. Slater, Eur. Phys. J. E **25**, 17 (2008)
13. S. Guillouzic, G.W. Slater, Phys. Lett. A **359**, 261 (2006)
14. A. Lzmitli, D.C. Schwartz, M.D. Graham, J. de Pablo, J. Chem. Phys. **128**, 085102 (2008)
15. M. Fyta, S. Melchionna, S. Succi, E. Kaxiras, Phys. Rev. E **78**, 036704 (2008)
16. V.V. Lehtola, R.P. Linna, K. Kaski, Europhys. Lett. **85**, 58006 (2009)
17. K. Luo, T. Ala-Nissila, S.C. Ying, A. Bhattacharya, Phys. Rev. Lett. **99**, 148102 (2007)
18. K. Luo, T. Ala-Nissila, S.C. Ying, A. Bhattacharya **100**, 058101 (2008)
19. K. Luo, T. Ala-Nissila, S.C. Ying, A. Bhattacharya, Phys. Rev. E **78**, 061911 (2008)
20. K. Luo, T. Ala-Nissila, S.C. Ying, A. Bhattacharya **78**, 061918 (2008)
21. P.-G. de Gennes, *Scaling Concepts in Polymer Physics* (Cornell University Press, Ithaca, NY, 1979)
22. J.L.A. Dubbeldam, A. Milchev, V.G. Rostishiashvili, T.A. Vilgis, Phys. Rev. E **76**, 010191(R) (2007)
23. T. Ambjörnsson, R. Metzler, Phys. Biol. **1**, 77 (2004)
24. T. Ambjörnsson, M. Lomholt, R. Metzler, J. Phys. Cond. Mat. **17**, S3945 (2005)
25. T. Ambjörnsson, R. Metzler, Phys. Rev. E **72**, 030901(R) (2005)
26. I.R. Epstein, Biophys. Chem. **8**, 327 (1978)
27. R.B. McQuistan, Nuovo Cimento **58**, 86 (1968)
28. P.L. Krapisky, E. Ben-Naim, J. Chem. Phys. **100**, 6778 (1994)
29. P.O. Luthi, J.J. Ramsden, B. Chopard, Phys. Rev. E **55**, 3111 (1997)
30. J. Talbot, G. Tarjus, P. Viot, J. Phys. A **32**, 2997 (1999)
31. W. Sung P.J. Park, Phys. Rev. Lett. **77**, 783 (1996)
32. M. Muthukumar, J. Chem. Phys. **111**, 10371 (1999)
33. J. Chuang, Y. Kantor, M. Kardar, Phys. Rev. E **65**, 011802 (2001)
34. K. Luo, T. Ala-Nissila, S.C. Ying, J. Chem. Phys. **124**, 034714 (2006)
35. I. Huopaniemi, K. Luo, T. Ala-Nissila, S.C. Ying, J. Chem. Phys. **125**, 124901 (2006)
36. D. Wei, W. Wang, X. Jin, Q. Liao, J. Chem. Phys. **126**, 204901 (2007)
37. A. Milchev, K. Binder, A. Bhattacharya, J. Chem. Phys. **121**, 6024 (2004)
38. R. Metzler, J. Klafter, Biophys. J. **85**, 2776 (2003)
39. R. Metzler, J. Klafter, Phys. Rep. **339**, 1 (2000)
40. Y. Kantor, M. Kardar, Phys. Rev. E **69**, 021806 (2004)
41. K. Luo, I. Huopaniemi, T. Ala-Nissila, S.C. Ying, J. Chem. Phys. **124**, 114704 (2006)

42. K. Luo, T. Ala-Nissila, S.C. Ying, A. Bhattacharya, J. Chem. Phys. **126**, 145101 (2007)
43. A. Bhattacharya, W.H. Morrison, K. Luo, T. Ala-Nissila, S.C. Ying, A. Milchev, K. Binder, Eur. Phys. J. E **29**, 423 (2009)
44. K. Luo, S.T.T. Ollila, I. Huopaniemi, T. Ala-Nissila, P. Pomorski, M. Karttunen, S.C. Ying, A. Bhattacharya, Phys. Rev. E **78**, 050901(R) (2008)
45. V.V. Lehtola, R.P. Linna, K. Kaski, Phys. Rev. E **78**, 061803 (2008)
46. M.G. Gauthier, G.W. Slater, J. Chem. Phys. **126**, 145101 (2007)
47. H. Vocks, D. Panja, G.T. Barkema, R.C. Ball, J. Phys. Cond. Matt. **20**, 095224 (2008)
48. J.L.A. Dubbeldam, A. Milchev, V.G. Rostiashvili, T.A. Vilgis, Europhys. Lett. **79**, 18002 (2007)
49. J.L.A. Dubbeldam, A. Milchev, V.G. Rostiashvili, T.A. Vilgis, J. Phys. Cond. Matt. **21**, 098001 (2009)
50. K. Luo, T. Ala-Nissilä, S.-Ch. Ying, R. Metzler, Europhys. Lett. **88**, 68006 (2009)
51. A. Yu. Grosberg, S. Nechaev, M. Tamm, O. Vasilyev, Phys. Rev. Lett. **96**, 228105 (2006)
52. T. Sakaue, Phys. Rev. E **76**, 021803 (2007)
53. M. Muthukumar, Phys. Rev. Lett. **86**, 3188 (2001)
54. K. Luo, R. Metzler, T. Ala-Nissila, S.-Ch. Ying, Phys. Rev. E **80**, 021907 (2009)
55. K. Luo, R. Metzler (unpublished)
56. K. Luo, R. Metzler, J. Chem. Phys. **133**, 075101 (2010)
57. K. Luo, R. Metzler, J. Chem. Phys. Rev. E **82**, 021922 (2010)
58. M.P. Allen, D.J. Tildesley, *Computer Simulation of Liquids* (Oxford University Press, 1987)